Physics Letters B 845 (2023) 138120

Contents lists available at ScienceDirect

Physics Letters B

journal homepage: www.elsevier.com/locate/physletb

Precise determination of quadrupole and hexadecapole deformation parameters of the *sd*-shell nucleus, ^{28}Si

Y.K. Gupta [a,b,*], V.B. Katariya [c], G.K. Prajapati [a], K. Hagino [d], D. Patel [c], V. Ranga [e], U. Garg [f], L.S. Danu [a,b], A. Pal [a], B.N. Joshi [a], S. Dubey [g], V.V. Desai [g], S. Panwar [e], N. Kumar [a], S. Mukhopadhyay [a], Pawan Singh [a,b], N. Sirswal [a], R. Sariyal [h], I. Mazumdar [g], B.V. John [a]

[a] Nuclear Physics Division, Bhabha Atomic Research Centre, Mumbai - 400085, India
[b] Homi Bhabha National Institute, Anushaktinagar, Mumbai 400094, India
[c] Department of physics, Sardar Vallabhbhai National Institute of Technology, Surat-395007, India
[d] Department of Physics, Kyoto University, Kyoto 606-8502, Japan
[e] Department of Physics, IIT Roorkee, Roorkee-247667, India
[f] Department of Physics and Astronomy, University of Notre Dame, Notre Dame, IN 46556, USA
[g] Tata Institute of Fundamental Research, Mumbai 400005, India
[h] Department of Physics, Panjab University, Chandigarh-160014, India

ARTICLE INFO

Article history:
Received 23 March 2023
Received in revised form 5 August 2023
Accepted 7 August 2023
Available online 11 August 2023
Editor: D.F. Geesaman

ABSTRACT

Quasi-elastic (QEL) scattering measurements have been performed using a ^{28}Si projectile off a ^{90}Zr target at energies around the Coulomb barrier. A Bayesian analysis within the framework of coupled channels (CC) calculations is performed in a large parameter space of quadrupole and hexadecapole deformations (β_2 and β_4) of ^{28}Si. Our results unambiguously show that ^{28}Si is an oblate shaped nucleus with β_2=-0.38 $\pm$ 0.01 which is in excellent agreement with results from electromagnetic probes. The sign and magnitude of quadrupole deformation along with a precise value of hexadecapole deformation (β_4=+0.03 $\pm$ 0.01) of ^{28}Si have been determined for the first time using QEL scattering. A remarkable agreement is obtained between the experimental and calculated β_4 values of ^{28}Si based on Skyrme-Hartree-Fock method. The present results demonstrate the strong sensitivity of the quasi-elastic scattering to the sign and magnitude to the ground state deformation parameters, thus affirming its suitability to be used for rare exotic nuclei using low intensity RIBs.

Nuclear deformation presents a fascinating example of a delicate balance between liquid drop nature and quantum many body aspects of the strongly interacting nucleons [1]. In the vicinity of the β-stability line, the nuclei close to the major shell closures exhibit spherical ground state shapes. While moving away from the shell closures, the shell structure of valence nucleons primarily governs the ground state shapes [2–4]. With the advent of RIB factories along with the associated development of more sophisticated experimental techniques and parallel advancement in modern theoretical frameworks, the shell structure evolution in the regions of extreme isospin, far from the valley of β-stability, is among the primary foci of current nuclear physics research [5].

Dominantly, the shell structure of valence nucleons leads to the axially symmetric deformations with reflection symmetry, namely the quadrupole and the hexadecapole [3]. The quadrupole deformation (β_2) is most commonly experienced as either elongated (prolate) or prostrated (oblate) shape. The value of β_2 is now being determined for many of the unstable nuclei [6], but, the higher order hexadecapole deformation (β_4) is not precisely known even for a majority of the stable deformed nuclei [7–10].

An island of deformed nuclei is known to exist in the *sd* shell region for the past several decades [11]. In this mass region, the sign of quadrupole deformation (prolate versus oblate) is ambiguous for many of the nuclei and the knowledge of the hexadecapole deformation is practically non-existent. In recent times, in connection with the N=28 shell quenching [12,13], a variety of calculations have been performed for nuclear deformation and its causes in the wide isotopic chains of Mg, Si, S, and Ar (*sd* and *fp* shells), employing different formalisms and density functionals [14–16]. These calculations predict a broad potential energy curve as a function of β_2 for the *sd* shell nuclei including the stables ones [17–21]. It is crucial to learn about the ground state shapes

* Corresponding author at: Nuclear Physics Division, Bhabha Atomic Research Centre, Mumbai - 400085, India.
E-mail address: ykgupta@barc.gov.in (Y.K. Gupta).

https://doi.org/10.1016/j.physletb.2023.138120

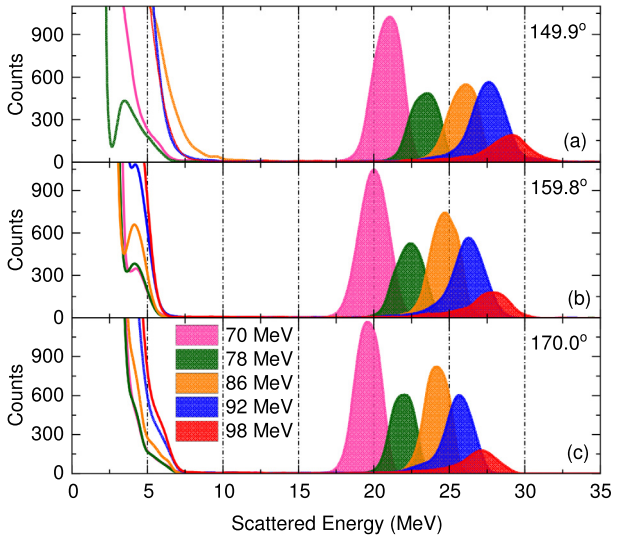

Fig. 1. Typical energy spectra of backward angle scattering at three laboratory angles and five typical beam energies. The filled curves in each panel beyond 15 MeV scattered energy, represent the QEL events. The events below 10 MeV are mostly due to the evaporated Light Charged Particles (LCPs).

in the stable region to examine the predictive power of modern theories for exotic nuclei being investigated at RIB factories, where beam intensity is a serious concern.

In case of the *sd* shell nucleus ^{28}Si, it has often been debated whether it is prolate- or oblate-shaped in its ground state. In several experiments, such as the inelastic scattering of neutrons [22], protons [23], deuterons [24]), and α particles [25], the scattering data have been explained by considering ^{28}Si as a prolate shaped nucleus. On the other hand, electromagnetic probes–electron scattering [26] and Coulomb excitation [27]–show it to be an oblate nucleus. There are also studies using the aforementioned mentioned inelastic scattering measurements which favor an oblate shape of ^{28}Si [28–30]. On the theoretical front as well, different theories predict conflicting quadrupole shapes, varying from oblate to prolate, with generally no predictions about the hexadecapole deformation [15,18,19]. Given this situation, it is crucially important to unambiguously determine whether ^{28}Si is oblate- or prolate-shaped in its ground state. In addition, its β_4 value determined so far also varies over a quite large range.

During the heavy-ion fusion, the coupling of internal degrees of freedom of the fusing nuclei, such as vibrational (spherical), rotational (deformed), and particle transfer, gives an opportunity to gain insight about the nuclear structure [31,32] from the measured Fusion Barrier Distributions (FBDs). The backward-angle QEL scattering provides an alternate route to get a good representation of FBD with some additional advantages [33]. Following the above idea, the sensitivity of the Quasi-elastic (QEL) scattering measurements to the ground state deformations including the higher order hexadecapole was demonstrated earlier in the heavy mass region (rare earths) [34]. Recently, it has been extended to the lighter mass region (*sd* shell region) [7]. A very precise value of hexadecapole deformation was obtained for ^{24}Mg which is a well established prolate-shaped nucleus [7]. It was pointed out that backward-angle QEL scattering could be used for unstable exotic nuclei.

Incidentally, most deformed nuclei happen to be prolate and only a few nuclei in the entire chart of stable nuclei are oblate in their ground states. The origin of the dominance of prolate over oblate shape is not fully understood, however. Therefore, before extending the QEL probe to short-lived exotic nuclei, we believe it is absolutely necessary to demonstrate that this probe is highly sensitive to the sign of quadrupole deformation (prolate versus oblate)

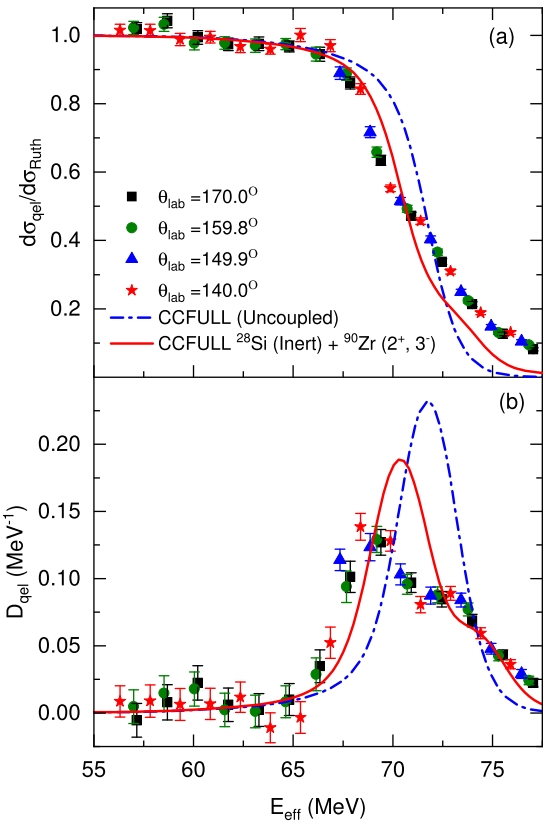

Fig. 2. Quasi-elastic excitation function (panel (a)) and extracted barrier distribution (panel (b)) at four backward angles for ^{28}Si + ^{90}Zr reaction. The dash-dotted and solid lines represent CCFULL calculations without including any coupling (uncoupled) and with including vibrational couplings of ^{90}Zr (2$^+$, 3$^-$), respectively.

in the lighter mass region where channel couplings are relatively weak. With this primary objective, we have measured backward angle QEL scattering of ^{28}Si off a ^{90}Zr target. In the present Letter, results obtained on ground state β_2 and β_4 values for ^{28}Si nucleus are presented. The present work unambiguously shows that ^{28}Si is an oblate nucleus in its ground state, with precise values of β_2 and β_4 obtained by performing Bayesian analysis in a large parameter space (from oblate to prolate). Thus, the present results affirm the suitability of backward angle QEL scattering as a potential probe for shorter-lived exotic nuclei using low intensity RIBs.

Quasi-elastic measurements were carried out using ^{28}Si DC beam from BARC-TIFR 14 MV Pelletron accelerator facility. Highly enriched (>95%) ^{90}Zr (150 μg/cm^2) deposited in oxide form on ^{12}C (40 μg/cm^2) was used as the target. It was prepared by the Center for Accelerator Target Science (CATS) at the Argonne National Laboratory. Quasi-elastic events were detected using thin Silicon Surface Barrier (SSB) detectors. Two SSB detectors (each of 15 μm) were placed at 170.0° on either side of the beam direction. One each SSB detector was placed at 140.0°(25 μm), 149.9° (25 μm), and 159.8°(15 μm) with respect to the beam direction. The angular opening of each detector was restricted to close to ±1°. Two more SSB detectors (1 mm), were mounted at 20.0° in the reaction plane on either side of the beam direction for the purpose of Rutherford normalization. Each of these monitor detectors had a collimator of 1 mm diameter. Rutherford scattering peak of ^{90}Zr was well separated from that of the ^{12}C (backing) and ^{16}O (target is ZrO_2) at forward angles (±20°).

Beam energies were used in the range of 70 to 102 MeV in steps of 2-MeV. At every change of beam-energy, the transmission of the beam was maximized through a collimator of 5 mm diameter, enabling a halo-free beam. The solid-angle ratios of mon-

itor to back-angle thin detectors were experimentally determined from Rutherford scattering of ^{28}Si projectile off ^{197}Au (150 μg/cm^2) target at 70 and 72 MeV beam energies. The quasi-elastic events consist of elastic and inelastic scattering from projectile and/or target excitations and to some extent from transfer events. The QEL events stopped within the thin SSB detectors placed at the backward angles. Owing to high negative Q-values in ^{28}Si+^{90}Zr reaction, the contribute from transfer channels in QEL events must be very negligible. In any case, all the QEL events dominantly comprise Projectile Like Fragments (PLFs), stopped within the thin SSBs, were clearly separated from evaporated Light Charged Particles (LCPs) from pulse height analysis. Typical energy spectra of backward angle scatterings are shown in the Fig. 1 at laboratory angles of 149.9°, 159.8°, and 170.0° for five typical beam energies. In each panel of the Fig. 1, the filled curves beyond 15 MeV scattered energy, represent the QEL events. The events below 10 MeV are mostly due to the evaporated LCPs. The two-body kinematics did not allow to have any contribution to the QEL events from ^{12}C and ^{16}O, present in the target. Among quasi-elastic events, the elastic events were dominant. All the SSB detectors were energy calibrated using elastic peaks of different beam energies. Successive changes in the kinetic energies of elastic events with varying beam energy, as seen in the Fig. 1 are observed to be in agreement with two-body kinematics at all the angles in going from 140° to 170°, which further benchmarked the identification of quasi-elastic events. The beam energies were corrected for energy loss in the half-thickness of the target.

Differential cross section for quasi-elastic events at each beam energy was normalized with Rutherford scattering cross section. The center-of-mass energy ($E_{\mathrm{c.m.}}$) was corrected for centrifugal effects at each angle as follows [33,35,36]:

$$E_{\mathrm{eff}} = \frac{2E_{\mathrm{c.m.}}}{(1+\mathrm{cosec}(\theta_{\mathrm{c.m.}}/2))} \tag{1}$$

where $\theta_{\mathrm{c.m.}}$ is the center-of-mass angle. The quasi-elastic excitation function for the ^{28}Si + ^{90}Zr reaction is shown in the Fig. 2(a) at the four backward angles. It is seen that the quasi-elastic excitation functions at multiple laboratory angles join quite smoothly. Quasi-elastic barrier distribution D_{qel} (E_{eff}) from quasi-elastic excitation function was determined using the relation [33,35]:

$$D_{qel}(E_{\mathrm{eff}}) = -\frac{d}{dE_{\mathrm{eff}}}\left(\frac{d\sigma_{\mathrm{qel}}}{d\sigma_{\mathrm{R}}}\right), \tag{2}$$

where $d\sigma_{\mathrm{qel}}$ and $d\sigma_{\mathrm{R}}$ are the differential cross sections for the quasi-elastic and Rutherford scatterings, respectively. A point difference formula is used to evaluate the barrier distribution, with the energy step of 2 MeV in the laboratory frame of reference. Similar to the excitation functions, the barrier distributions determined from excitation functions at multiple laboratory angles joins quite smoothly as shown in the Fig. 2(b). The smooth joining of the data in excitation function as well as the derived barrier distribution, ensures correct identification of the quasi-elastic events. It is to be noted that unlike that in ^{16}O and ^{24}Mg [7], a prominent "shoulder" is observed in the higher energy region of the barrier distribution (see Fig. 2(b)) in case of ^{28}Si scattering off the same target, ^{90}Zr. The origin of this "shoulder" is discussed later in the text.

Coupled channels (CC) calculations were carried out using a modified version of CCFULL code [37] for quasi-elastic scattering (see Ref. [7] for details). The CC calculations were carried out at first without including any channel coupling. These uncoupled CC calculations are represented by the dash-dotted lines in Figs. 2(a) and (b). It is clearly seen that uncoupled calculations cannot reproduce the experimental data. The CC calculations were then extended to include the vibrational couplings of the target, ^{90}Zr,

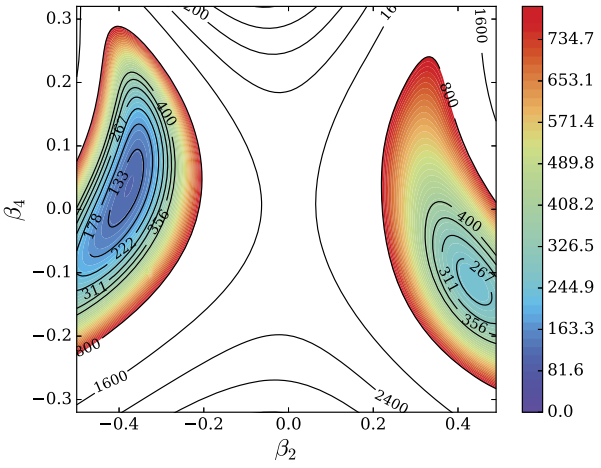

Fig. 3. A χ^2 distribution in the two dimensional space of β_4 and β_2 of ^{28}Si, determined by comparing experimental QEL excitation function with CC calculations (see text).

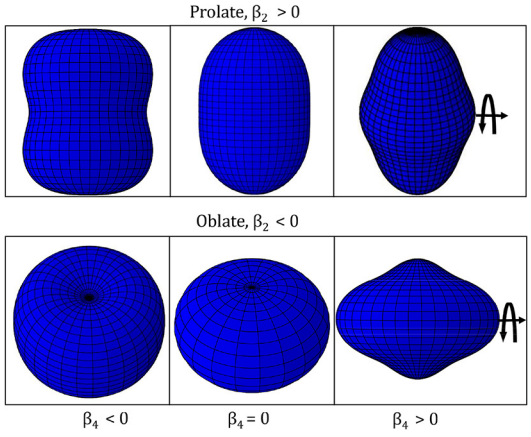

Fig. 4. Schematic shapes: top row for prolate ($\beta_2 > 0$) and bottom row for oblate ($\beta_2 < 0$) quadrupole deformation with positive and negative values of hexadecapole deformation (β_4).

while the projectile nucleus, ^{28}Si was assumed to be inert. The vibrational quadrupole (2^+) state at 2.19 MeV and the octupole (3^-) state at 2.75 MeV of ^{90}Zr, were taken into account. The coupling strengths, β_2^{vib} and β_3^{vib} for the above 2^+ and 3^- states of ^{90}Zr were used as 0.089 and 0.211, respectively, as determined earlier [7]. It is clearly seen that the CC calculation only with the vibrational couplings of ^{90}Zr deviates significantly from experimental data, pointing to the need to include other degrees of freedom of either projectile or the target within the CCFULL framework.

^{28}Si shows a rotational band built on the ground state [38] with a non-zero quadrupole moment, $Q(2^+)$ [39]. These features suggest the importance of including the rotational couplings of ^{28}Si within the CC calculations in order to reproduce the quasi-elastic excitation function and the barrier distribution for ^{28}Si + ^{90}Zr reaction. Along with quadrupole deformation, the hexadecapole deformation in the ground state of ^{28}Si was also included in the CC calculations. Rigid rotor model was used for this purpose. In order to reproduce the experimental data and determine precise values of β_2 and β_4, the CC calculations were carried out in a large parameter space of quadrupole and hexadecapole deformations. The parameters β_2 and β_4 were varied in the range of -0.5 (oblate) to $+0.5$ (prolate) and -0.4 to $+0.4$, respectively with a step size of 0.01 for both. Coulomb and nuclear parts for both quadrupole and hexadecapole deformations were kept at same values. The first three rotational states of ^{28}Si, namely, 0^+, 2^+, and 4^+, were in-

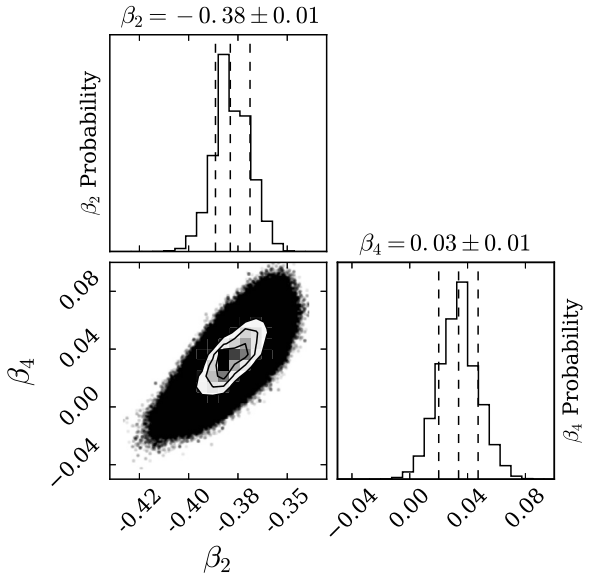

Fig. 5. Two-dimensional probability distributions of β_2 and β_4 for ^{28}Si, resulting from the MCMC simulation [7] from the experimental data (see text). Plus- and minus-uncertainties are shown.

cluded in the CCFULL calculations; the coupling to the 6^+ state is found to give a negligible contribution. Large number of CC calculations were performed using the "ANUPAM" supercomputer of Bhabha Atomic Research Centre.

The prominent "shoulder" as shown in the Fig. 2(b) originates primarily from vibrational couplings in ^{90}Zr. The couplings becomes stronger with increasing charge product of the projectile and the target nuclei. In case of ^{16}O, the coupling is not strong enough, and the shoulder originating only from the ^{90}Zr excitations is not resolved in the barrier distribution. On the other hand, for ^{24}Mg, one can see a less pronounced "shoulder" at around 67 MeV of E_{eff} in the Fig. 3 of the Ref. [7]. In addition to the vibrational couplings of ^{90}Zr, the asymmetric barrier distribution is obtained due to the reorientation term for the rotational couplings in the projectile, *viz.* the coupling from the first 2^+ state to the same 2^+ state of the deformed projectile. The effect of the reorientation term on the shape of the barrier distribution depends on various factors such as the excitation energy of the 2^+ state, the charge product of the projectile and target nuclei, and relative sign of β_2 and β_4 as discussed in detail in Ref. [40].

Further, a χ^2 was calculated between the experimental QEL scattering excitation function and CC calculations including vibrational couplings of ^{90}Zr and rotational couplings of ^{28}Si for each combination of β_2 and β_4 using following equation;

$$\chi^2(\beta_2, \beta_4) = \sum_{i=1}^{N} \frac{[Y_i - f(\beta_2, \beta_4)]^2}{\sigma_i^2} \tag{3}$$

where Y_i represents the experimental value of the excitation function at the i^{th} energy point, σ_i is the uncertainty in the data, and $f(\beta_2, \beta_4)$ represents corresponding CCFULL calculation for a particular combination of β_2 and β_4. In Eq. (3), the summation runs over all the data points (N) in the effective energy (E_{eff}) range of 64 to 75 MeV. The χ^2-distribution thus obtained in the two-dimensional space of β_4 and β_2 is shown in Fig. 3. It shows two minima, one corresponding to oblate (left contour) and the other to prolate shape (right contour). The χ^2-value corresponding to the oblate shape is approximately four times smaller than that for prolate shape as can be seen from the Fig. 3. Thus, the χ^2 distribution reveals an oblate ground state shape of ^{28}Si with a

Table 1
Quadrupole and hexadecapole deformation of ^{28}Si using different experimental probes. Results of theoretical calculations based on Skyrme-Hartree-Fock (SHF) methods [41] are also shown.

Experiment	β_2	β_4
Present work	−0.38±0.01	+0.03±0.01
(CE[1]) [27]	−0.39	
(e, e′) [26]	−0.39	+0.10
(n, n′) [28]	−0.39	
(n, n′) [42]	−0.48	0.15
(n, n′) [42]	−0.42 ±0.02	+0.20 ± 0.05
(n, n′) [22]	+0.41	
(p, p′) [29]	−0.34	+0.25
(p, p′) [43]	−0.55	+0.33
(p, p′) [23]	+0.41	
(d, d′) [24]	+0.45	
(α, α') [25]	+0.36	
(α, α') [30]	−0.32 ± .01	+0.08±0.01
(^{16}O, ^{16}O′) [44]	−0.34	
Theory		
SHF-SV-min [45]	−0.327	+0.035
SHF-SV-bas [46]	−0.334	+0.041
SHF-SLy4 [47]	−0.333	+0.047

[1] Coulomb Excitation.

certain non-zero value of the hexadecapole deformation. In order to visualize oblate and prolate shapes with positive and negative hexadecapole deformations, schematic shapes were generated, as shown in Fig. 4, using the following expression [8] for nuclear radius in a "PYTHON" script;

$$R(\theta, \phi) = R_o \left[1 + \beta_2 Y_2^0(\theta, \phi) + \beta_4 Y_4^0(\theta, \phi)\right], \tag{4}$$

where, Y_2^0 and Y_4^0 are the spherical harmonics for L=2 and 4, respectively. The radius parameter R_o is varied in such a way that the volumes of the prolate and oblate shapes remain the same as that of the spherical nucleus. One can notice from Fig. (4), a dramatic change in the shape of a nucleus with changing signs of β_2 and β_4.

In order to obtain the quantitative values of β_2 and β_4 for ^{28}Si and their associated uncertainties from present data of quasi-elastic excitation function, a Bayesian analysis with a Markov-Chain Monte Carlo (MCMC) framework was carried out in the parameter range of −0.5 to 0 and −0.4 to +0.4 for β_2 and β_4, respectively, which correspond to the global minimum. The aforementioned χ^2 distribution simultaneously constrains the likelihood function, which is defined as [7].

$$P(\vec{Y}|\beta_2, \beta_4) = \exp\left(-\chi^2/2\right). \tag{5}$$

The likelihood function is a conditional probability density of a dataset, $\vec{Y}$, given some values for the model parameters β_2, β_4. In turn, the inverse conditional probability, $P(\beta_2, \beta_4|\vec{Y})$ yields information on the distribution of β_2 and β_4 given a set of data. The connection between these two probability distributions is encapsulated within Bayes' Theorem:

$$P(\beta_2, \beta_4|\vec{Y}) = \frac{P(\vec{Y}|\beta_2, \beta_4) P(\beta_2, \beta_4)}{P(\vec{Y})}, \tag{6}$$

where, $P(\vec{Y})$ and $P(\beta_2, \beta_4)$ are, respectively, the so-called prior distributions of $\vec{Y}$ and (β_2, β_4) which were merely taken to be uniform distributions over the parameter space (see Ref. [7] for further details).

Probability distributions obtained from the Bayesian analysis corresponding to the global minimum (oblate) in the χ^2-distribution are shown in Fig. 5. The β_2 and β_4 are moderately correlated with a correlation of $\sim +0.138$, which is evidenced

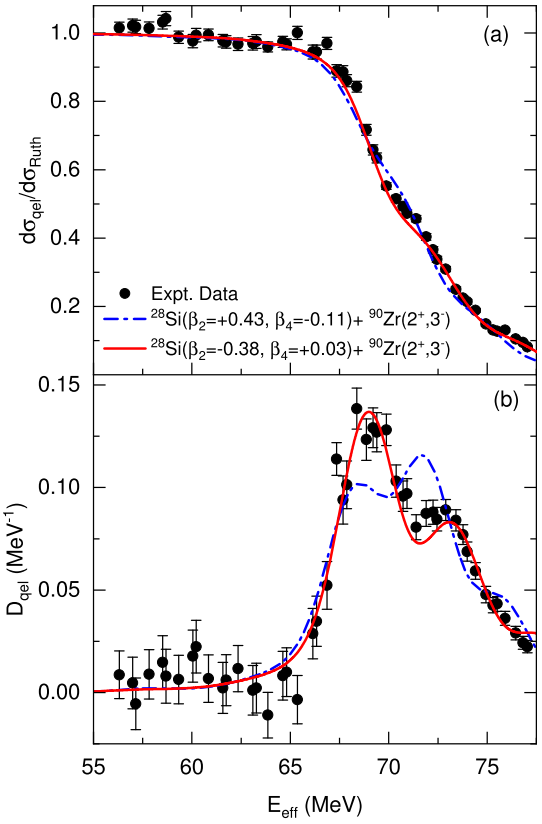

Fig. 6. Quasi-elastic excitation function (panel (a)) and derived barrier distribution (panel (b)) for ^{28}Si + ^{90}Zr reaction. The dash-dotted (blue) and solid lines (red) show CC calculations for the two parameter sets, corresponding to prolate and oblate shapes, respectively. Vibrational couplings of ^{90}Zr (2^+, 3^-) were included (see text).

graphically within the two-dimensional probability distribution shown in Fig. 5. Examination of the projections of the probability density onto the parameter axes yields extracted values of $\beta_2 = -0.38 \pm 0.01$ and $\beta_4 = +0.03 \pm 0.01$, with approximately symmetric distributions centered at the medians. The Bayesian analysis is repeated in the parameter space, β_2= 0 to +0.5 and β_4=-0.4 to +0.4 which correspond to the shallow minimum in the prolate region of the χ^2-distribution (see Fig. 3); it yields $\beta_2 = +0.43 \pm 0.01$ and $\beta_4 = -0.11 \pm 0.01$.

Experimental data for quasi-elastic excitation function and derived barrier distribution are compared with CC calculations using the β_2 and β_4 parameters of ^{28}Si, determined using the Bayesian analysis corresponding to oblate as well as prolate regions and the results are presented in Fig. 6. The quasi-elastic excitation function (Fig. 6 (a)) does not show a huge difference between the prolate and oblate shapes. However, the derived barrier distribution, which provides a finger-print of the structure of fusing partners, exhibits an enlarged sensitivity with the two parameter sets, as depicted in the Fig. 6(b). One can see that the agreement between CC calculations with the oblate shape of ^{28}Si and the experimental data is excellent, whereas the calculations corresponding to the prolate shape deviate from the data quite significantly. Thus, Bayesian analysis carried out in the present work for QEL scattering data shows that ^{28}Si is uniquely an oblate shaped in its ground state having $\beta_2 = -0.38 \pm 0.01$. Moreover, it also yields a precise value of hexadecapole deformation, $\beta_4 = +0.03 \pm 0.01$.

The β_2 and β_4 values of ^{28}Si have been reported in literature from the measurements of inelastic scattering off electron, proton, neutron, deuteron, α, ^{16}O, and Coulomb excitation (CE). These values are listed in the Table 1. One can see that previously reported ground state β_2 values of ^{28}Si vary in a quite wide range alongwith its sign from prolate (+ve) to oblate (-ve). However, the electromagnetic probes, Coulomb excitation and electron scattering have been the primary tools to estimate the nuclear size and shapes. The β_2 value and its sign for ^{28}Si determined in present work show excellent agreement with those determined using electromagnetic probes (see Table 1). Apparently, Coulomb excitation and electron scattering do not show a good sensitivity to hexadecapole deformation. The β_4 of ^{28}Si reported earlier varies quite significantly from +0.08 to +0.33. It is the first time that β_4 of ^{28}Si has been determined precisely to be +0.03±0.01 along with a precise β_2 value and its sign having good overlap with those determined using electromagnetic probes (see Table 1).

Table 1 also shows the calculation results of the Axial Hartree-Fock + BCS code SkyAx for three different parameter sets, SLy4 [47], SV-min [45], and SV-bas [46]. The deformation parameters β_2 and β_4 are evaluated with the calculated Q_2 and Q_4 moments by taking into account the non-linear terms of the deformation parameters. Even though the absolute values of β_2 are somewhat smaller than the value obtained in this analysis, it is remarkable that the sign and the value of β_4 are consistent with the present results.

In summary, quasi-elastic measurements have been carried out in the ^{28}Si+^{90}Zr reaction at multiple laboratory angles. Quasi-elastic excitation functions and barrier distributions derived therefrom have been compared with the Coupled Channels (CC) calculations using CCFULL code. Considering ^{28}Si as an inert nucleus, and taking into account only vibrational couplings of ^{90}Zr, the calculations deviate significantly from the experimental data. In further CC calculations including rotational couplings of ^{28}Si, the quadrupole deformation was varied in a large parameter range from oblate to prolate (β_2 from -0.5 to $+0.5$). Along with quadrupole, the hexadecapole deformation was varied in a wide range (β_4 from -0.4 to $+0.4$). A Bayesian analysis was carried out to determine the best choice of ground state β_2 and β_4 values for ^{28}Si. Following all these analyses, ^{28}Si is determined to be an oblate-shaped nucleus with rather precise values of $\beta_2 = -0.38 \pm 0.01$ and $\beta_4 = +0.03 \pm 0.01$, respectively. The β_2 value for ^{28}Si, and its sign, obtained in the present work is in excellent agreement with the previously reported values from electromagnetic probes–electron-scattering and Coulomb excitation. Unambiguous determination of the sign and precise values for the quadrupole and hexadecapole deformations for this *sd*-shell nucleus, has been achieved for the first time using QEL scattering. The sign and value of the experimental β_4 show a remarkable agreement with those calculated using the Skyrme-Hartree-Fock methods. Thus, the present results affirm quasi-elastic scattering as a potential route to investigate the ground state structure of exotic nuclei using RIBs where beam intensity is of primary concern. We point out here that among all the probes to determine the ground state deformation of a short lived exotic nucleus, quasi-elastic scattering and Coulomb excitations are the ones where the exotic nuclei can be used in the form of a beam bombarding an appropriate stable target. However, the ease of performing "singles" measurements in quasi-elastic scattering, makes it somewhat superior to the Coulomb excitation.

We are thankful to Dr. B. K. Nayak, Dr. V. Jha, and Dr. R. K. Choudhury for discussion at various stages of this work. Authors are also thankful to Mr. Raman Sehgal and Mr. Vaibhav Kumar for helping with the "ANUPAM" supercomputing facility of BARC. We are grateful to the operating staff of BARC-TIFR Pelletron for the smooth operation of the machine. YKG is thankful to Mrs. Aditi Kulkarni and Ms. Shreya Walavalkar for extending their help during the experiment and preparation of the figures for the current manuscript. UG acknowledges the support from U.S. National Science Foundation (Grant No. PHY-2011890).

Declaration of competing interest

The authors declare the following financial interests/personal relationships which may be considered as potential competing interests:

U. Garg reports financial support was provided by National Science Foundation (Grant No. PHY-2011890).

Data availability

Data will be made available on request.

References

[1] A. Bohr, B.R. Mottelson, Nuclear Structure: Volume II (Nuclear Deformations), 1975.
[2] R.F. Casten, Nuclear Structure from a Simple Perspective, Oxford University Press, 2001.
[3] R.S. Mackintosh, Rep. Prog. Phys. 40 (1977) 731.
[4] Michael Bender, Paul-Henri Heenen, Paul-Gerhard Reinhard, Rev. Mod. Phys. 75 (2003) 121.
[5] Takaharu Otsuka, Alexandra Gade, Olivier Sorlin, Toshio Suzuki, Yutaka Utsuno, Rev. Mod. Phys. 92 (2020) 015002.
[6] T. Glasmacher, Annu. Rev. Nucl. Part. Sci. 48 (1998) 1.
[7] Y.K. Gupta, B.K. Nayak, U. Garg, K. Hagino, K.B. Howard, N. Sensharma, M. Şenyiğit, W.P. Tan, P.D. O'Malley, M. Smith, Ramandeep Gandhi, T. Anderson, R.J. deBoer, B. Frentz, A. Gyurjinyan, O. Hall, M.R. Hall, J. Hu, E. Lamere, Q. Liu, A. Long, W. Lu, S. Lyons, K. Ostdiek, C. Seymour, M. Skulski, B. VandeKolk, Phys. Lett. B 806 (2020) 135473.
[8] F.S. Stephens, R.M. Diamond, J. de Boer, Phys. Rev. Lett. 27 (1971) 1151.
[9] W. Brückner, D. Husar, D. Pelte, K. Traxel, M. Samuel, U. Smilansky, Nucl. Phys. A 231 (1974) 159.
[10] G. Kaur, K. Hagino, N. Rowley, Phys. Rev. C 97 (2018) 064606.
[11] R.W. Ibbotson, T. Glasmacher, B.A. Brown, L. Chen, M.J. Chromik, P.D. Cottle, M. Fauerbach, K.W. Kemper, D.J. Morrissey, H. Scheit, M. Thoennessen, Phys. Rev. Lett. 80 (1998) 2081.
[12] A. Gade, B.A. Brown, J.A. Tostevin, D. Bazin, P.C. Bender, C.M. Campbell, H.L. Crawford, B. Elman, K.W. Kemper, B. Longfellow, E. Lunderberg, D. Rhodes, D. Weisshaar, Phys. Rev. Lett. 122 (2019) 222501.
[13] Y. Suzuki, M. Kimura, Phys. Rev. C 104 (2021) 024327.
[14] D.D. Dao, F. Nowacki, Phys. Rev. C 105 (2022) 054314.
[15] T.R. Werner, J.A. Sheikh, M. Misu, W. Nazarewicz, J. Rikovska, K. Heeger, A.S. Umar, M.R. Strayer, Nucl. Phys. A 597 (1996) 327.
[16] Michael Bender, Paul-Henri Heenen, Phys. Rev. C 78 (2008) 024309.
[17] A. Gaamouci, I. Dedes, J. Dudek, A. Baran, N. Benhamouda, D. Curien, H.L. Wang, J. Yang, Phys. Rev. C 103 (2021) 054311.
[18] Myaing Thi Win, K. Hagino, Phys. Rev. C 78 (2008) 054311.
[19] A. Li, X.R. Zhou, H. Sagawa, Prog. Theor. Exp. Phys. 6 (2013) 063D03.
[20] P. Kumar, V. Thakur, S. Thakur, V. Kumar, S.K. Dhiman, Acta Phys. Pol. B 52 (2021) 401.
[21] H. Mei, K. Hagino, J.M. Yao, T. Motoba, Phys. Rev. C 97 (2018) 064318.
[22] R. De Leo, G. ÓErasmo, E.M. Fiore, A. Pantaleo, M. Pignanelli, Phys. Rev. C 20 (1979) 1244.
[23] R.K. Cole, C.N. Waddell, R.R. Dittman, H.S. Sandhu, Nucl. Phys. 75 (1966) 241.
[24] H. Niewodniczański, J. Nurzyński, A. Strzałkowski, J. Wilczyński, J.R. Rook, P.E. Hodgson, Nucl. Phys. 55 (1964) 386.
[25] J. Kokame, K. Fukunaga, N. Inoue, H. Nakamura, Phys. Lett. 8 (1964) 342.
[26] Y. Horikawa, Y. Torizuka, A. Nakada, S. Mitsunobu, Y. Kojima, M. Kimura, Phys. Lett. B 36 (1971) 9.
[27] G.C. Ball, O. Häusser, T.K. Alexander, W.G. Davies, J.S. Forster, I.V. Mitchell, J.R. Beene, D. Hörn, W. Mclatchie, Nucl. Phys. A 349 (1980) 271.
[28] J. Böttcher, H. Blank, E. Finckh, C. Forstner, W. Jaumann, G. Schall, H. Scheuring, U. Schneidereit, K.S. Tauber, A. Weipert, W. Tornow, E. Woye, J. Phys. G 9 (1983) L65.
[29] R. de Swiniarski, C. Glashausser, D.L. Hendrie, J. Sherman, A.D. Bacher, E.A. McClatchie, Phys. Rev. Lett. 23 (1969) 317.
[30] H. Rebel, G.W. Schweimer, G. Schatz, J. Specht, R. Löhken, G. Hauser, D. Habs, H. Klewe-Nebenius, Nucl. Phys. A 182 (1972) 145.
[31] M. Dasgupta, D.J. Hinde, N. Rowley, A.M. Stefanini, Annu. Rev. Nucl. Part. Sci. 48 (1998) 401.
[32] K. Hagino, N. Takigawa, Prog. Theor. Phys. 128 (2012) 1061.
[33] E. Piasecki, Ł. Świderski, P. Czosnyka, M. Kowalczyk, K. Piasecki, M. Witecki, T. Czosnyka, J. Jastrzebski, A. Kordyasz, M. Kisieliński, T. Krogulski, M. Mutterer, S. Khlebnikov, W.H. Trzaska, K. Hagino, N. Rowley, Phys. Lett. B 615 (2005) 55.
[34] H.M. Jia, C.J. Lin, F. Yang, X.X. Xu, H.Q. Zhang, Z.H. Liu, Z.D. Wu, L. Yang, N.R. Ma, P.F. Bao, L.J. Sun, Phys. Rev. C 90 (2014) 031601(R).
[35] H. Timmers, J.R. Leigh, M. Dasgupta, D.J. Hinde, R.C. Lemmon, J.C. Mein, C.R. Morton, J.O. Newton, N. Rowley, Nucl. Phys. A 584 (1995) 190.
[36] B.K. Nayak, R.K. Choudhury, A. Saxena, P.K. Sahu, R.G. Thomas, D.C. Biswas, B.V. John, E.T. Mirgule, Y.K. Gupta, M. Bhike, H.G. Rajprakash, Phys. Rev. C 75 (2007) 054615.
[37] K. Hagino, N. Rowley, A. Kruppa, Comput. Phys. Commun. 123 (1999) 143.
[38] National Nuclear Data Center (NNDC), Nuclear, Science References (version of 2015) information extracted from the NSR database, http://www.nndc.bnl.gov/ensdf/.
[39] N.J. Stone, At. Data Nucl. Data Tables 1 (2016) 111.
[40] V.B. Katariya, Y.K. Gupta, et al., to be published.
[41] P.-G. Reinhard, B. Schuetrumpf, J.A. Maruhn, Comput. Phys. Commun. 258 (2021) 107603.
[42] G. Haouat, Ch. Lagrange, R. de Swiniarski, F. Dietrich, J.P. Delaroche, Y. Patin, Phys. Rev. C 30 (1984) 1795.
[43] A.G. Blair, C. Glashausser, R. de Swiniarski, J. Goudergues, R. Lombard, B. Mayer, J. Thirion, P. Vaganov, Phys. Rev. C 1 (1970) 444.
[44] A. Dudek-Ellis, V. Shkolnik, D. Dehnhard, Phys. Rev. C 18 (1978) 1039.
[45] J. Erler, C.J. Horowitz, W. Nazarewicz, M. Rafalski, P.-G. Reinhard, Phys. Rev. C 87 (2013) 044320.
[46] P. Klüpfel, P.-G. Reinhard, T.J. Bürvenich, J.A. Maruhn, Phys. Rev. C 79 (2009) 034310.
[47] E. Chabanat, P. Bonche, P. Haensel, J. Meyer, R. Schaeffer, Nucl. Phys. A 635 (1998) 231.